TU Delft

Delft University of Technology

Development and testing of an active trailing edge morphing demonstrator for a rotary wing

Zahoor, Yasir; Sodja, Jurij; De Breuker, Roeland; Voskuijl, Mark

DOI
10.1115/SMASIS2021-67590

Publication date
2021

Document Version
Accepted author manuscript

Published in
Proceedings of ASME 2021 Conference on Smart Materials, Adaptive Structures and Intelligent Systems, SMASIS 2021

Citation (APA)
Zahoor, Y., Sodja, J., De Breuker, R., & Voskuijl, M. (2021). Development and testing of an active trailing edge morphing demonstrator for a rotary wing. In *Proceedings of ASME 2021 Conference on Smart Materials, Adaptive Structures and Intelligent Systems, SMASIS 2021* Article V001T05A005 (Proceedings of ASME 2021 Conference on Smart Materials, Adaptive Structures and Intelligent Systems, SMASIS 2021). The American Society of Mechanical Engineers (ASME). https://doi.org/10.1115/SMASIS2021-67590

Important note
To cite this publication, please use the final published version (if applicable).
Please check the document version above.

Copyright
Other than for strictly personal use, it is not permitted to download, forward or distribute the text or part of it, without the consent of the author(s) and/or copyright holder(s), unless the work is under an open content license such as Creative Commons.

Takedown policy
Please contact us and provide details if you believe this document breaches copyrights.
We will remove access to the work immediately and investigate your claim.

This work is downloaded from Delft University of Technology.
For technical reasons the number of authors shown on this cover page is limited to a maximum of 10.

Proceedings of The ASME 2021 Conference on Smart Materials, Adaptive Structures and Intelligent Systems
SMASIS 2021
September 14-15, 2021, Virtual, Online

SMASIS2021-67590

DEVELOPMENT AND TESTING OF AN ACTIVE TRAILING EDGE MORPHING DEMONSTRATOR FOR A ROTARY WING

Yasir Zahoor, Jurij Sodja, Roeland De Breuker
Faculty of Aerospace Engineering
Delft University of Technology
Delft, The Netherlands

Mark Voskuijl
Faculty of Military Sciences
Netherlands Defence Academy
Den Helder, The Netherlands

ABSTRACT

This paper discusses the development and whirl tower testing of an active translation induced camber morphing system for rotorcraft. The system deploys the morphing flap based on the amplitude and type of the input signal. As a case study, a demonstrator is developed and tested primarily under the centrifugal force generated by a whirl tower setup. The actuation system consists of amplified piezoelectric actuators, while the morphing skin is made out of carbon fiber prepreg composite material. The response of the morphing skin and the actuators is measured and compared to the numerical studies used to design the morphing demonstrator. Results indicate that the response of the active system, including the actuators and the flexible skin, matches well to those predicted during the numerical studies. The outcome of these studies shows that the system has the potential to be used for the primary control of the rotorcraft if operated at 1/revolution or for mitigating noise and vibration if operated at 2/revolution or higher frequencies. Subsequently, the concept can be integrated into a Mach-scaled rotor blade which can be tested under both aerodynamic and centrifugal loads to further assess its performance.

ACRONYMS

APA Amplified Piezoelectric Actuator.
CG Center of Gravity.
COR Center of Rotation.
DT Displacement Transducer.
FP Fixed Point.
LED Light Emitting Diode.
RF Reaction Force.
RP Reference Point.
RPM Revolution Per Minute.
TRIC Translation Induced Camber.

INTRODUCTION

Modern rotorcraft are noisy, full of vibration, and aerodynamically inefficient. To improve on these aspects morphing devices can be used. The morphing capability in an aircraft can be achieved in an active and passive way. An active actuation system works by using specific actuators for controlling the behavior of the morphing control surface. In such cases, both the input and output are continuously monitored and controlled through a feedback system. Most of the work in the morphing domain is based on active morphing systems both for fixed-wing aircraft and rotorcraft [1]. It must be noted that irrespective of the type of aircraft, the biggest current design problem seems to be to combine properties like flexibility and stiffness into one structure. Due to this reason, the level of maturity of morphing skins is generally low [2].

While implementing a morphing scheme, some concepts require sufficient space and design changes for the idea to work. One such example is the use of telescopic wing that resulted in an increase in the lift to drag ratio [3]. However, as noted by the researchers during the experiments of the telescopic wing, the overall performance benefits are reduced due to the drag penalty

imposed by the seams of the wing sections. On the other hand, when the modifications are limited to only those sections where the high lift system is located, the necessity of design change is limited, and the performance benefits are enhanced [4]. In other words, by incorporating design changes in leading edge and trailing edge portions, major modifications in wings may be avoided, reducing the overall development time significantly. Regarding the scale of modifications, it has been shown for fixed-wing aircraft that camber modifications may require minimal changes. At the same time, such modifications provide means for a sufficient increase in wing performance [5]. Monner et al. showed that the chordwise camber variation leads to an improvement in operational flexibility and performance [4]. In a similar work for helicopters [6], the option of smart trailing edge flap was studied and showed significant improvements in the helicopter performance.

A morphing system in a rotorcraft can be envisaged for requirements such as the primary control or noise and vibration mitigation. For the primary control, conventional rotorcraft are generally equipped with swashplates which have proved to be highly reliable. However, this traditional arrangement of rotor primary control adversely affects the performance of the rotorcraft. This is because these swashplates are mechanically complex, have numerous exposed linkages, bearings, pushrods, and hinges, which contribute to helicopter aerodynamic drag [7]. This problem can be resolved by incorporating the control mechanisms embedded in the rotor blades making it an active area of research. Exploring a solution for the primary control, Shen et al. showed that the trailing edge flaps are capable of performing both primary flight control and active vibration control functions [8]. In their study, the required trailing edge flap angles were found to be moderate if a proper selection of rotor blade-pitch index angle is made.

The other area of interest in the rotorcraft community is the reduction in noise and vibration of rotorcraft to improve the overall performance. Both noise and vibration are associated with the main rotor, tail rotor, and engines, with the main rotor being the primary source, especially in forward flight [9]. A contributing factor to the noise is the Blade Vortex Interaction (BVI). BVI arises from the interaction of the rotor blade with the tip vortices generated by previous rotor blade passages creating an unstable aerodynamic load and leads to undesirable noise effects and fatigue in the rotor blade structure [10].

To overcome the issue of noise and vibration in the main rotor, two approaches are well known, i.e., the Higher Harmonic Control (HHC) and the Individual Blade Control (IBC). HHC systems are realized by using an additional mechanical system of pushrods connected to a conventional swashplate causing additional tilt of its plane with higher frequencies [11]. In the case of an IBC system, each rotor blade is controlled individually by pitch-link actuators or servo-flaps [12]. However, it has been shown that using IBC, simultaneous control of both noise and vibration may be achieved [13, 14]. Such a concept was also flight tested in the BK117 S7045 experimental helicopter, equipped with an active rotor blade system based on piezoelectrically driven trailing edge flaps [14].

In terms of the actuation scheme, two different actuator concepts have been proposed in the literature. One approach uses active materials directly bonded or embedded in a rotor blade to twist the entire lifting surface. A different approach for developing rotating frame actuators uses discrete actuators fixed within the contour of the rotor blade to control a trailing edge servo flap [15]. While several actuation concepts for deforming helicopter rotor blades have been studied in the past, the main focus has remained on the active twist, and camber variations [16]. In the case of airfoil camber variation, the trailing edge morphing concept is generally preferred. This is because it offers advantages of a possible modular design, simplified maintenance, and the fact that the actuator may be easily detached from the host rotor blade structure for replacement [16].

Trailing edge camber morphing is traditionally linked to the servo flap in rotorcraft. The earliest example of a servo flap appeared during the early 1920s when Louis Brennan worked on a helicopter concept that had unusually large single two-bladed rotor and servo-flaps for control [17]. In 1930, Corradino d'Ascanio of Italy built a helicopter with servo tabs shown in Fig. 1.

FIGURE 1. CORRADINO D'ASCANIO'S HELICOPTER WITH SERVO TABS.

Later in the 1940s, Charles Kaman (Kaman Helicopters) designed a helicopter with servo-flaps [18]. When these flaps were deflected cyclically, the aerodynamic moments caused the rotor blades to twist, changing their angle of attack and thus introducing a cyclic rotor control capability [17]. This servo-flap shown in Fig. 2 is considered a trademark of the Kaman Helicopters to date.

The use of a trailing edge flap for primary flight control appears attractive in the context of an actively controlled rotor, where the embedded flaps can perform multiple functions [8]. In

FIGURE 2. FLAP USED IN KAMAN HELICOPTERS.

one case, a comprehensive rotorcraft analysis for a swashplateless rotor with trailing edge flaps was developed, and the actuation requirements of a primary control system were evaluated. The swashplateless rotor was shown to be trimmed successfully with the trailing edge flap control system in the complete range of advance ratios [19]. In a swashplateless electrically controlled rotor, primary flight control can be provided by applying rotor blade pitch inputs via an integrated active trailing edge flap enabling the possibility to achieve, in principle, any form of the control input theoretically [20].

The trailing edge camber morphing idea stems from the concept of plain servo flap. Unlike the traditional hinged-flap that are externally mounted aft of the rotor blade's trailing edge, plain flaps eliminate the hinge gap and flap support structure. This brings advantages of reduced power losses due to less aerodynamic drag and improved flap effectiveness. For rotorcraft, trailing edge camber morphing provides an opportunity to improve these plain flaps by eliminating the hinge and giving a smooth surface [21].

While designing a trialing edge morphing system, the frequency of morphing actuation is highly dependent on the desired goal. For instance, the performance and power benefits are achieved from quasi-static to 2/rev inputs [22], vibration reduction from N+/-1 inputs (where N is the number of rotor blades) [23], and noise mitigation from considerably higher frequencies [24]. Active vibration control can be achieved by changing the aerodynamic loads on the airfoil through high-frequency changes in camber [25].

From the research work in the past, it is clear that active control and noise and vibration mitigation are possible by employing servo flaps. Trailing edge morphing flaps offer similar capabilities with the added benefits of smooth shape changes resulting in enhanced performance. However, in terms of the design of the flap and its actuation, the challenges are complex, and the implementation has mostly remained limited [26]. This is mainly because of the conflicting requirements of weight, strength, and flexibility imposed by a morphing solution [27]. To increase the concept to the realization ratio of morphing solutions, conventional materials and structures can be used. This can be done if the key requirements of strength and flexibility are achieved without a significant weight penalty. An example of such a concept for a fixed-wing aircraft is the so-called Translation Induced Camber (TRIC) [28]. This concept can introduce uniform or differential camber (twist) over the span of the morphing section. In addition, it relies on utilizing conventional aircraft structures and materials for morphing purposes; thus, in essence, it has the potential to fulfill the conflicting requirements of lightweight, flexibility, and strength at the same time. In the present work, the same concept as shown in Fig. 3 has been used for morphing rotorcraft flaps. For this purpose, Amplified Piezoelectric Actuators (APA) developed by CEDRAT Technologies are used [29].

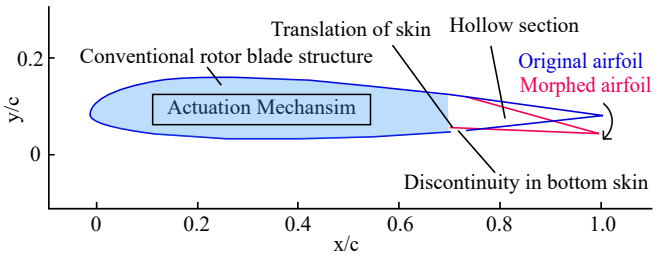

FIGURE 3. TRIC CONCEPT FOR ROTORCRAFT.

In order to show the effectiveness of the concept, an elementary model is developed to test the concept on a whirl tower setup. The model used for whirl tower testing is solely to investigate the response of the actuation system and the morphing flap under the centrifugal force, while the aerodynamic loads are not assessed during this campaign. For this reason, the demonstrator is intentionally designed with a blunt face, making it possible to minimize the aerodynamic effects on the morphing flap. Consequently, the test and analysis do not intend to quantify the control power. The maximum flap deflection angle to be achieved during this study is set between 6° to 8°. The definition of the deflection angle θ is shown in Fig. 4, where θ is the angle corresponding to a line passing through the undeformed chord line at a distance equal to the flap chord length. It is considered +ve downwards.

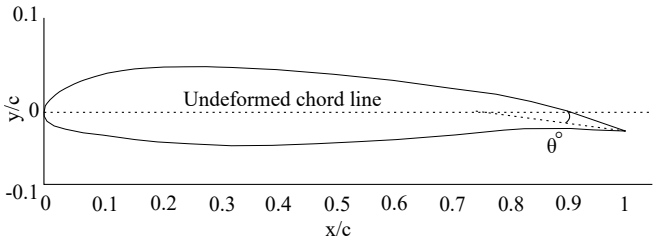

FIGURE 4. DESCRIPTION OF DEFLECTION ANGLE.

This paper presents an overview of the development of the whirl tower demonstrator and explains the results and validation in the end. The discussion in this paper is organized as follows. First, the demonstrator design is introduced with emphasis on morphing skin and actuator selection and the role of the numerical model. Afterward, the focus shifts to the test campaign in which the test objectives, setup, and instrumentation are discussed. This is followed by the results obtained for quasi-static and dynamic testing and a comparison with the numerical work. In the end, conclusions and recommendations for future work are presented.

DEMONSTRATOR DESIGN

The demonstrator design mainly includes the characterization of flexible skin, actuator selection, and design of overall actuation system.

Flap Skin Design and Actuator Selection

For the skin design and calculation of actuator force and stroke, a numerical model is developed in Abaqus, which consists of a portion of flap based on NACA 23102 with a chord length of c = 270 mm. The flap chord is selected as 24% of the chord length. The boundary conditions used on the flap are shown in Fig. 5. The element size for the mesh is selected as 5 mm after doing a mesh convergence study. The portion of the top skin which is fixed to the rotor blade structure is constrained in all degrees of freedom. The bottom skin, which translates in the chordwise direction, is constrained in the out-of-plane direction. A reference point (RP) is created at the location where the skin is attached to the actuator and is constrained using a coupling constraint to the bottom portion of the skin. A displacement is applied in the chordwise direction, and reaction force (RF) is noted at RP. By applying appropriate displacements with regards to the actuator stroke, corresponding tip deflections of the flap and RF are recorded. The RF estimated numerically serves as the maximum force required by the actuator to deflect the flap based on the worst-case load scenario. It must be noted that when the aerodynamic force is also considered, its effect is included either by calculating the flap hinge moment [30] or by transferring the forces from the Computational Fluid Dynamics (CFD) simulations to the Finite Element Analysis (FEA) [31].

The most important consideration of a morphing skin is that it should be able to provide strength and flexibility in the direction of actuation at the same time. Out of several options considered during the design phase, prepreg composite material (NTPT-HTS(12K)-5-35%) is used due to the high stiffness to weight ratio and in-house availability. The Prepreg material is a thermoplastic-toughened epoxy resin unidirectional (UD) carbon fiber Prepreg system [32]. The fabricated skin for the demonstrator is a quasi-isotropic laminate having seven layers [+45/-45/90/0/90/-45/+45], where 0° corresponds to the chordwise direction.

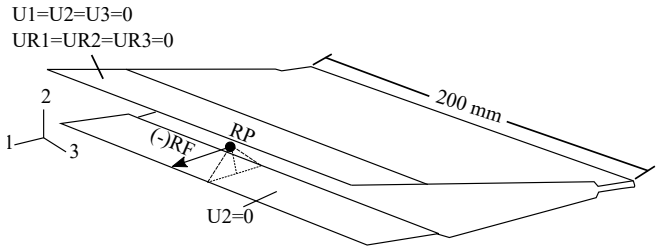

FIGURE 5. FLAP BOUNDARY CONDITIONS.

Based on the skin analysis, APA 1500L is selected to test the active concept. The main considerations behind this selection are as follows:

1. The actuators can be housed inside the prescribed volume.
2. The actuators are able to produce sufficient stroke that can result in a flap deflection of 6° to 8°.
3. The actuators are able to operate at high frequencies.

The piezoelectric actuators are inherently limited in providing the stroke. To overcome this issue, two actuators are used in series. Such an arrangement does not affect the blocked force of the actuators but doubles the magnitude of the resulting stroke. The main properties of APA 1500L actuators are shown in Tab. 1.

TABLE 1. CHARACTERISTICS OF APA 1500L [29]

.

Parameter	Value	Unit
Nominal stroke	1480	μm
Blocked force	99	N
Voltage range	-20 .. +150	V
Stiffness	0.0669	N/μm
Mass	143	grams
Force/Volt	0.588	N/V

For the present test campaign, the actuators are operated at a maximum positive voltage of 140 V to get a flap deflection of around 6° to 8°. Fig. 6 shows the operating range of these actuators in terms of stroke and force. It also highlights the point where maximum force to deflect the flap (obtained numerically) is indicated.

Equation 1 represents the characteristic equation in terms of applied voltage, stroke, and blocked force [33]. This equation is

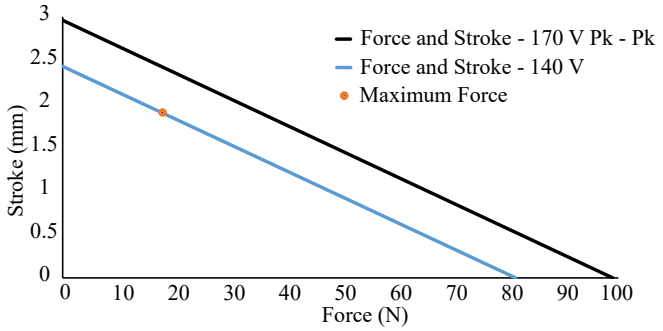

FIGURE 6. APA 1500L ACTUATOR OPERATING RANGE.

used to determine the ideal stroke by using the estimated force magnitude from the numerical analysis.

$$\frac{F}{F_{max}} + \frac{X}{X_{max}} = \frac{V}{V_{max}} \tag{1}$$

Actuation System Design

The main purpose of the active morphing concept demonstrator is to capture the response of the skin and actuators under centrifugal loads. The details of the actuation system are shown in Fig. 7. Since the aerodynamic forces on the flap are not considered for this elementary model, the rotor blade section is not made in a typical airfoil shape. Consequently, the aluminum housing for the actuation system is simplified for manufacturing. Two APA, connected in series, are attached to the flap by steel link rods resulting in the actuation mechanism of the flap.

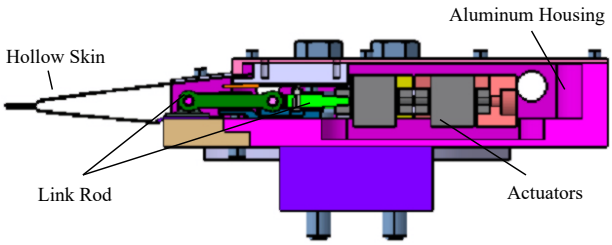

FIGURE 7. CROSS-SECTION OF THE ACTUATION SYSTEM.

When a rotor blade rotates, both the flap and actuators experience components of centrifugal force, which acts on a line passing through the center of rotation (COR) and the center of gravity (CG) of the mass (m). It is represented by the following equation.

$$F = m \cdot r \cdot \omega^2 \tag{2}$$

The CG of the actuation system is adjusted with respect to the COR in such a way that the chordwise component of centrifugal force becomes negligible and neglected for both the actuators and flap. This signifies the fact that the selection of actuators is mainly governed by the aerodynamic and elastic forces on the flap. In addition, with reference to Eq. 2, for a portion of a hollow and thin skin of composite material acting as a flap, the longitudinal (spanwise) component is also negligible if the skin is lightweight and appropriately constrained to the rigid structure. The effect of this component on the actuator and associated mechanics can be minimized by having additional supports. This is achieved in two ways, as shown in Fig. 8. Two thin blades made of steel are included in the assembly. These blades are fastened at one end with the actuators and are clamped at the other end with the aluminum structure. This puts the blades under tension when the centrifugal force is applied and prevents the actuators from undergoing bending. The second support is provided in the form of teflon pads, which sandwich the link rods during the movement. These teflon pads cause low friction while at the same time provide requisite support to the link rods.

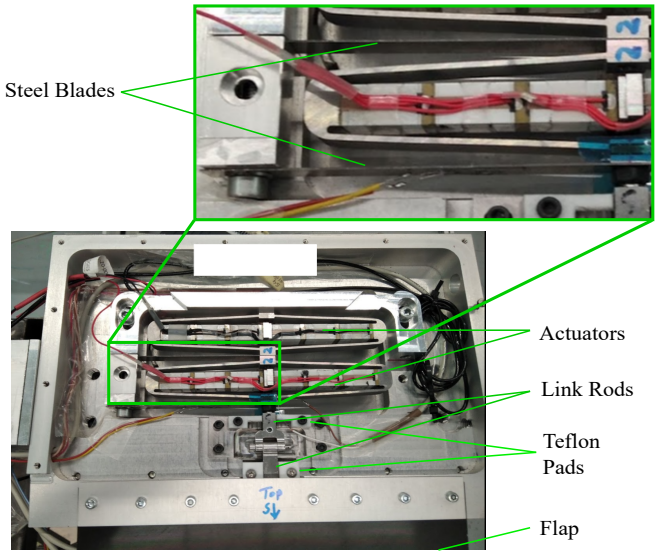

FIGURE 8. COMPONENTS OF THE ACTUATION SYSTEM.

The complete CAD model of the demonstrator is shown in Fig. 9. The actuation system is attached to the aluminum housing

using an aluminum base plate. This plate is then inserted inside the hollow aluminum beam (4x4 mm aluminum channel) and is secured using a nut and bolt combination. At the other end, a counterweight is secured to balance the demonstrator about its center of rotation. The central interface part, made of aluminum, is also secured inside the aluminum channels on both sides.

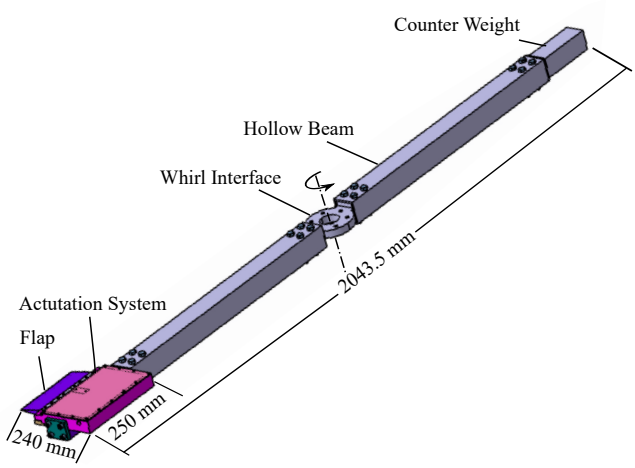

FIGURE 9. CAD MODEL OF THE DEMONSTRATOR.

TEST CAMPAIGN

The test campaign involves testing the active morphing demonstrator under centrifugal loads. One of the main objectives of the test was to record the response of the actuator under centrifugal load by recording the stroke. The second main objective was to observe the tip deflections of the flap. The measurements corresponding to these objectives were recorded in both the quasi-static and dynamic tests of the actuation system.

Test Setup

The test setup shown in Fig. 10 consists of an active morphing system demonstrator with an interface at the center for its attachment to the whirl tower. The whirl tower system is mounted on a rigid base. A data acquisition system is used to record the corresponding measurements while a high-speed camera (Photron [1] FASTCAM Mini AX200) is positioned to capture the tip deflection of the flap.

Whirl Tower Description. The whirl tower setup shown in Fig. 10 is used as a test rig for the vertical axis wind turbine [34]. It consists of thrust bearings that transfer the thrust and

[1]https://photron.com/

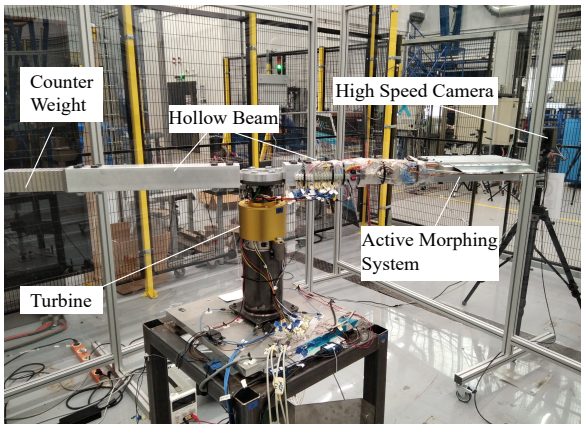

FIGURE 10. WHIRL TOWER SETUP.

weight of the rotor to the structural base while allowing the rotation and torque to be passed through a torque and speed sensor. The drive-line is further extended to a motor that is coupled to an appropriate gearhead to increase the torque. The full whirl tower system is clamped to a heavy steel base that is placed on the ground. Considering the limitations of the whirl tower, the maximum allowable limit for the test campaign is set as 240 RPM.

Instrumentation

The types of sensors used in the experiments and their location are shown in Tab. 2.

TABLE 2. INSTRUMENTATION.

Sensor	Location
Strain gauge	Top skin surface
Strain gauge	Bottom skin surface
Strain gauge	Actuator
Displacement transducer	Link rod
LEDs	01 on skin tip, 04 on aluminum housing, 01 fixed to ground
Triaxial Accelerometer	Whirl tower base

The strain gauge used on the top skin is a quarter bridge strain gauge mounted in the chordwise direction. This strain gauge is placed approximately at the midpoint, both spanwise and chordwise, and is used to measure the strains when the skin

bends or morphs as a result of the applied force. Another strain gauge is placed on the bottom skin in the spanwise direction to observe the strains that might occur as the result of centrifugal force. The third strain gauge is a full-bridge strain gauge that comes embedded on the piezoelectric actuator. A displacement transducer (SoftPot from *spectrasymbol* [2]) is used to measure the stroke of the actuation system. This transducer is in the form of a membrane over which a spring-loaded plunger moves. This plunger is screwed to the link rod which is attached to the skin.

The purpose of mounting a triaxial accelerometer on the base of the whirl tower is to monitor any adverse vibrations on the demonstrator during the whirl tower testing.

In order to capture the tip displacement of the flap from the high-speed camera, a single LED is placed on the tip of the flap to indicate its deflection under different actuation amplitudes. In addition, one LED is set as a fixed point (FP) attached to the ground while four LEDs are placed on the aluminum housing to indicate any torsional deformations of the demonstrator. These four LEDs are on the same plane. This arrangement of LEDs is shown in Fig. 11.

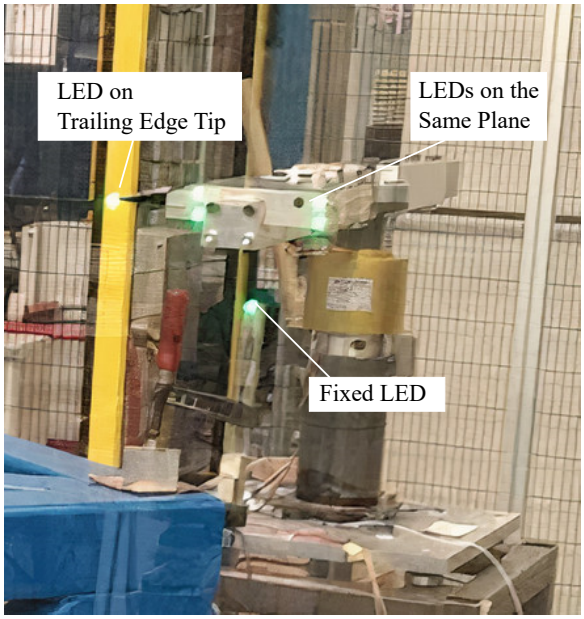

FIGURE 11. WHIRL TOWER SETUP WITH LEDs.

To minimize the background effect and to record the frames at high RPM, the frame rate is set to 9000 frames/s, and shutter speed is adjusted to $1/6e5$ s. For each test case, high-speed video is recorded by triggering the camera at a point where the plane defined by 4 LEDs as shown in Fig. 11 is nearly perpendicular to the viewing axis of the camera. This triggering is generated by a photosensor present in the whirl tower and enables the recording of the frames before and after the trigger generation. This ensures that the frame of interest is always captured and also helps to reduce the number of frames captured in each video.

TEST RESULTS AND DISCUSSION

Before commencing the testing, a comparison between the response of the strain gauge mounted on the piezoelectric actuator to the displacement transducer (DT) is carried out. Since the DT is farthest in the actuation chain, it is used for the correlation with the numerical studies. Fig. 12 shows the correlation of the two sensors at no load. There is slight variation in the two outcomes mainly because of the difference in types and functionality of the two sensors and also due to the difference in calibration technique.

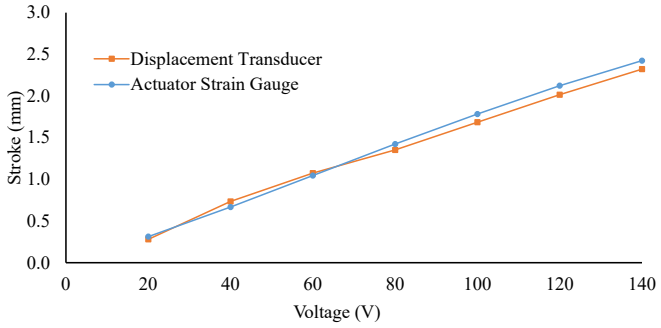

FIGURE 12. COMPARISON OF STROKES AT NO-LOAD.

As mentioned previously in the demonstrator design discussion that two blades are used to support the bending of the actuators under centrifugal forces. In order to ascertain the effect of these blades on the force and stroke, analysis is carried out in Abaqus and shown in Fig. 13. In this case, the blades are deflected by applying a unit force, and the resulting tip deflection is noted. From this analysis, the force/stroke for the blades is noted as 1.6 N/mm. The ideal case in Fig. 14 represents the stroke obtained by using the appropriate values in Eq. 1 and compared to the stroke from DT. This shows that for a maximum deflection, the force consumed by the blades is approximately 4% of the available blocked force.

Once the flap is integrated and the actuation mechanism is complete, the response of the ideal case and the actual case are compared. For the ideal case (based on Eq. 1), the force/stroke is obtained from Abaqus and turns out to be 6.14 N/mm. The results in Fig. 15 show that the response of the skin is not entirely linear. Here also, the two curves show a good match and the response of the DT is also mostly linear.

[2]https://www.spectrasymbol.com/

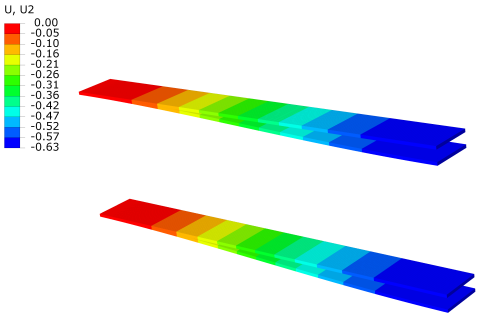

FIGURE 13. DEFLECTION OF BLADES.

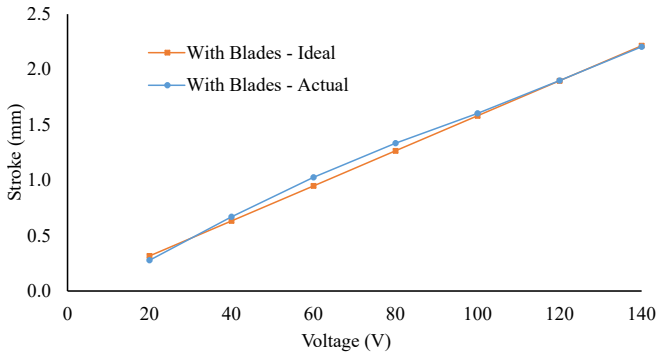

FIGURE 14. STROKE OF ACTUATORS WITH BLADES.

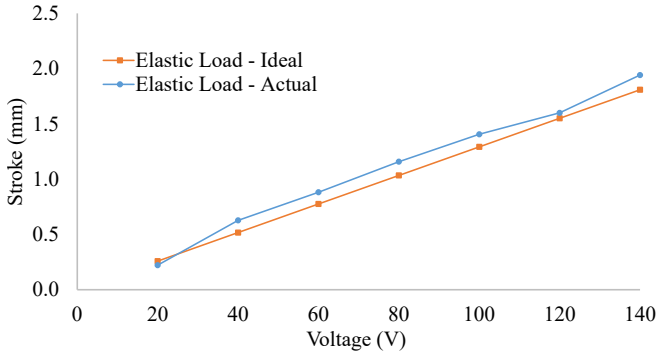

FIGURE 15. STROKE OF ACTUATORS WITH FLAP.

Quasi-Static Testing

During this testing, the demonstrator is rotated at a maximum allowable speed of 240 RPM. However, this is done sequentially in four steps starting from 60 RPM and then testing at 120 RPM, 180 RPM, and 240 RPM. This is done to avoid any potential issues with the setup. At every RPM, the flap is deflected by varying the voltage supplied to the actuators from 20 V to 140 V. A typical signal given to the actuators is shown in Fig. 16 in which the rise time of each input signal is reduced with the corresponding increase in RPM.

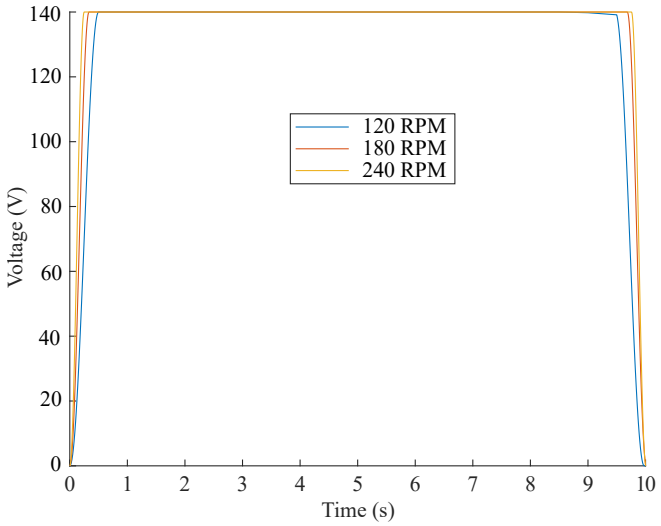

FIGURE 16. INPUT SIGNAL (140 V) AT DIFFERENT RPM.

The response of actuators (displacement measured by DT) corresponding to the input signals in Fig. 16 is shown in Fig. 17. As indicated, the actuator response is quite consistent in terms of achieving the desired stroke.

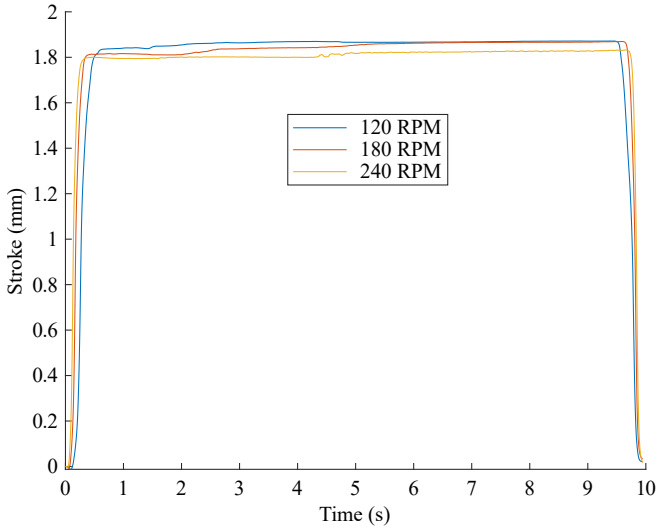

FIGURE 17. RESPONSE (140 V) AT DIFFERENT RPM.

Fig. 18 shows the effect of the RPM on the actuator stroke recorded in Fig. 17. It can be observed that the maximum degradation in the stroke is only around 3.5% against a centrifugal force of approximately 50 g's experienced by the actuation system.

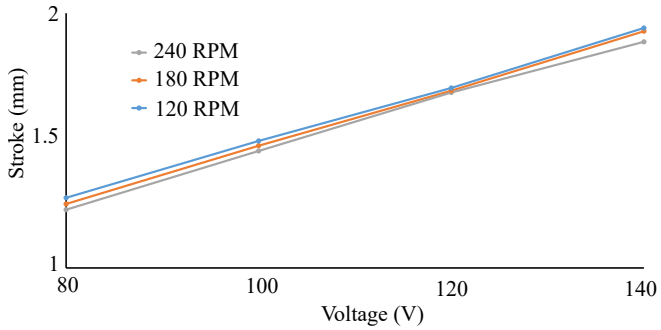

FIGURE 18. EFFECT OF RPM ON STROKE.

The numerical strain on the top skin for the maximum stroke of 2.4 mm is shown in Fig. 19. The overall strain levels are quite low, and the strain in the vicinity of the location of the strain gauge is in the range of 600 to 650 $\mu\varepsilon$.

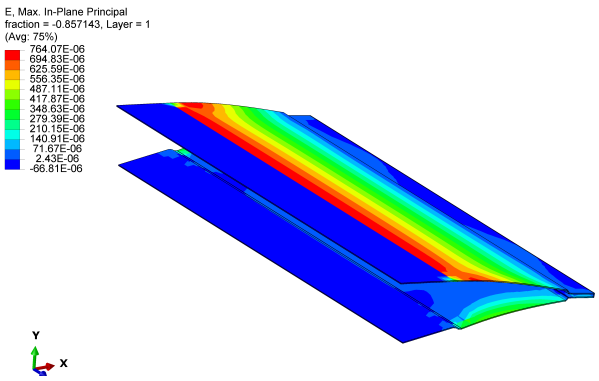

FIGURE 19. STRAIN IN TOP SKIN AT MAXIMUM DEFLECTION.

Figure 20 shows the response of the strain gauge at 0 RPM and 240 RPM. It indicates that the strains predicted by the numerical model are quite close to the actual strains measured by the strain gauge. It also indicates that the chordwise component of the centrifugal force has no effect on the strains. The strain gauge bonded on the skin to measure the influence of the spanwise component of the centrifugal force does not present any significant strains indicating that the effect of the centrifugal force is not evident in the morphing skin used in this demonstrator.

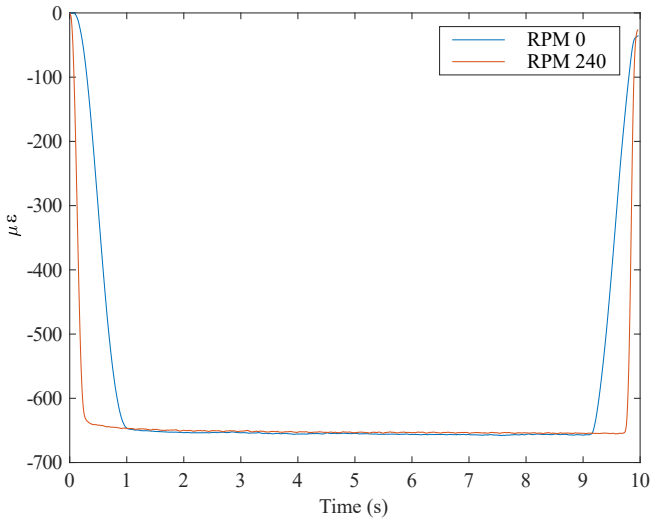

FIGURE 20. STRAIN TOP SKIN AT 0 AND 240 RPM.

Throughout the testing, the response of the triaxial accelerometer was monitored, and no significant levels of vibrations were observed, which indicates that the whole test setup was well balanced.

As mentioned earlier, a high-speed camera is used to capture the tip deflection. Figure 21 shows two images captured using the high-speed camera at the undeformed position and maximum deflected position when the rotor blade is rotated at 240 RPM.

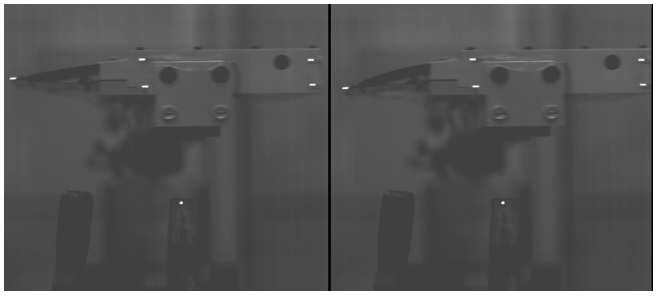

FIGURE 21. IMAGES AT 240 RPM.

A Matlab routine is created to post-process the images and obtain the tip deflection with respect to FP. Figure 22 shows the tip deflection obtained at 240 RPM and compares the results to

the tip deflection obtained in Abaqus by using the boundary conditions shown in Fig. 5. The results show quite a good correlation between the two sets of data points corresponding to various strokes when voltage is varied from 20 V to 140 V.

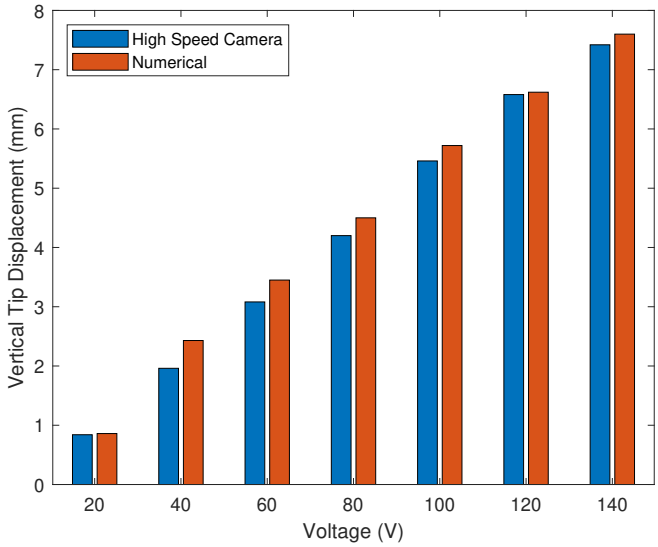

FIGURE 22. TIP DEFLECTION COMPARISON at 240 RPM.

Dynamic Testing

During the dynamic testing, the actuation is carried out at various frequencies related to the RPM. This testing is also carried out by gradually increasing the RPM from 60 to 240. Keeping in view a maximum RPM of 240 in perspective, the actuation frequencies are selected as 1/rev, 2/rev, and 3/rev with respect to each RPM. Since the peak to peak voltage range for the actuators lies between -20 V to +150 V, the input signal is generated in the form of a sine wave accordingly. Equation 3 shows how the input signal is generated, changing the frequency, voltage level, and offset.

$$V_i = V + \Lambda \cdot U \cdot sin(\omega \cdot t) \tag{3}$$

where V_i is the input voltage signal, V is the voltage level, U is the voltage offset, Λ is the amplitude shift factor (0 to 1) and ω is the frequency.

Using Eq. 3, a typical signal resembles the one as shown in Fig. 23. Similar signals are generated for frequencies up to 12 Hz, corresponding to 3/rev for a rotational speed of 240 RPM.

The response of the actuators is noted by recording the displacement of the DT. Figure 24 shows the actuator response at

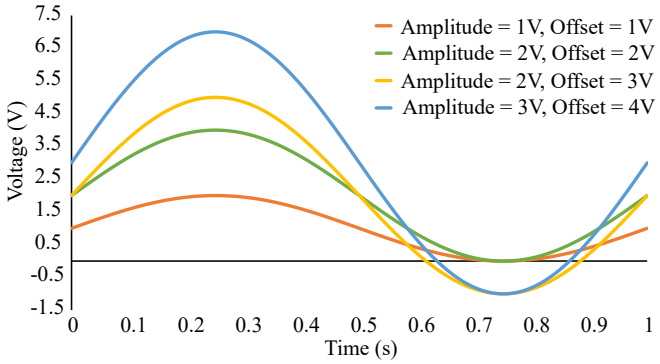

FIGURE 23. EXAMPLE OF INPUT SIGNAL AT 1 HZ.

12 Hz for a period of 1 s. This result indicates that actuators responded consistently to the input signal under dynamic conditions. More importantly, it demonstrates that the morphing flap is capable of operating at higher frequencies repeatedly. This outcome is of extreme importance for the applicability of the TRIC morphing concept in a rotorcraft application.

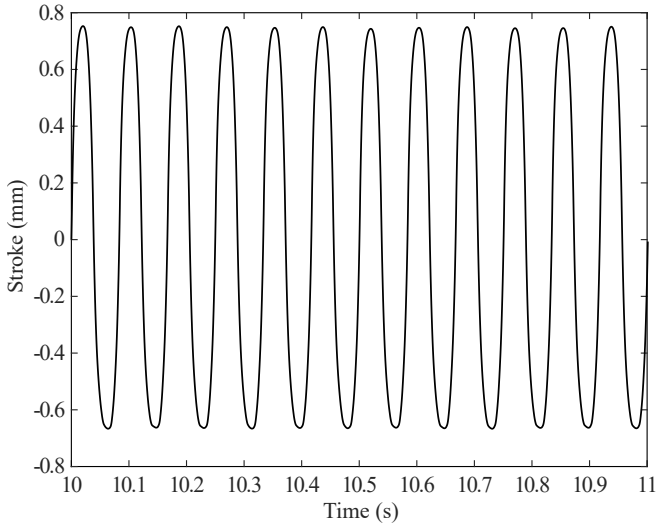

FIGURE 24. MEASUREMENT OF ACTUATOR STROKE: ACTUATOR AT 3/REV, ROTOR BLADE AT 240 RPM.

To further support the argument presented in the previous section, the images were captured using a high-speed camera for the dynamic case. Due to the slight difference in the rotational frequency of the demonstrator and the operating frequency of the flap, each revolution (rev) resulted in recording a different tip deflection. It was ensured that at least one cycle is captured during the whole recording phase to capture the flap response. The im-

ages are post-processed, and the responses are recorded. As an example, tip deflections against the highest input amplitude are shown in Fig. 25. A sine curve is fitted to the data with five terms using the sum of the sines model as represented by Eq. 4.

$$y = \sum_{i=1}^{n} a_i sin(b_i x + ci) \tag{4}$$

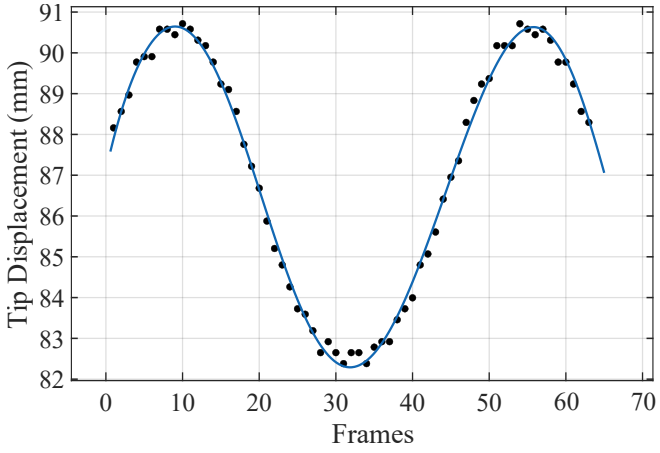

FIGURE 25. MEASUREMENT DYNAMIC RESPONSE THROUGH HIGH SPEED CAMERA.

Figure 25 shows that the curve fits the points data indicating the response of the flap matching to the input signal. It is also evident from the figure that the maximum tip displacement of approximately 8mm is more than the one shown in Fig. 22 and corresponds to the higher voltage input as shown in Fig. 23 for the 3 V amplitude case.

CONCLUSIONS

This paper presents the process of developing and testing an active morphing system for rotorcraft based on the translation induced camber. The tests are conducted on a whirl tower setup that can test the demonstrator under a centrifugal force of 50g's approximately. The results present a good comparison between numerical study and experimental campaign and show that the active system with piezoelectric actuators performs well under centrifugal forces. The degradation in the stroke is less than 4% for the maximum stroke case at 240 RPM. The strains in the skin are also low and have no change due to centrifugal forces showing that the overall actuation system, with mechanical blades and supports to resist bending, serves the purpose well. The effectiveness of support blades is prominent, which adds rigidity to the system without adding a significant penalty in stroke. The results indicate that the TRIC concept initially envisaged for the fixed-wing aircraft can be effectively used for the rotorcraft applications demanding higher operating frequencies.

The promising results obtained during the test campaign encourage the design of a Mach-scaled rotor that has a similar actuation system and is subjected to higher centrifugal loads coupled with aerodynamic loads. Such a test would be useful in establishing the performance of this active system in actual flight. After proper assessment of control power requirements, it can also be established whether the present concept is more suited for primary control or vibration and noise mitigation.

ACKNOWLEDGMENT

The research work is a part of the European Union project SABRE (Shape Adaptive Blades for Rotorcraft Efficiency) under Horizon2020.

REFERENCES

[1] Mistry, M., 2012. "Quasi-Static Rotor Morphing Concepts for Rotorcraft Performance Improvements".

[2] Thill, C., Etches, J., Bond, I., Potter, K., and Weaver, P., 2008. "Morphing skins". *Aeronautical Journal,* ***112***(1129), pp. 117–139.

[3] Blondeau, J., Richeson, J., Pines, D. J., and Norfolk, A., 2003. "Design , development and testing of a morphing aspect ratio wing using an inflatable telescopic spar". *44th AIAA / ASME / ASCE / AHS Structures , Structural,* ***1718***(April), pp. 1–11.

[4] Monner, H. P., Hanselka, H., and Breitbach, E. J., 1998. "Development and design of flexible Fowler flaps for an adaptive wing". *SPIE 3326, Smart Structures and Materials 1998: Industrial and Commercial Applications of Smart Structures Technologies, 60,* ***3326***(Cl), pp. 60–70.

[5] SZODRUCH, J., 1985. "The influence of camber variation on the aerodynamics of civil transport aircraft". *23rd Aerospace Sciences Meeting*.

[6] Garcia, E., 2002. "Smart structures and actuators: past, present, and future". pp. 1–12.

[7] Saxena, A., and Chopra, I., 2011. "Development and testing of a swashplateless rotor with compact brushless motor actuated flaps for primary control".

[8] Shen, J., Yang, M., and Chopra, I., 2006. "Swashplateless helicopter rotor with trailing-edge flaps for flight and vibration control". *Journal of Aircraft,* ***43***(2), pp. 346–352.

[9] Grohmann, B. A., Maucher, C., Prunhuber, T., Jänker, P., Dieterich, O., Enenkl, B., Bauer, M., Ahci, E., Altmikus, A., and Baier, H., 2008. "Multidisciplinary design and optimization of active trailing edge for smart helicopter rotor

blade". *Mechanics of Advanced Materials and Structures,* ***15***(3-4), pp. 307–324.

[10] Melnykowycz, M. "Active Airfoil Design and Finite Element Analysis of Smart Structures for Rotor Blade Applications".

[11] Miller, M., Narkiewicz, J., Kania, W., and Czechyra, T., 2006. "The application of helicopter rotor blade active control systems for noise and vibration reduction and performance improvement".

[12] Teves, D., Niesl, G., Jacklin, S., and Field, M., 1995. "The Role of Active Control in Future Rotorcraft".

[13] Jacklin, S. A., Blaas, A., Germany, K.-c., Teves, D., and Kube, R., 1995. "Consumption Through Individual Blade Control". pp. 662–680.

[14] Enenkl, B., 2006. "Dy 04 active rotor control by flaps for vibration reduction-full scale demonstrator and first flight test results".

[15] Prechtl, E. F., and Hall, S. R., 1997. "Design of a high-efficiency discrete servo-flap actuator for helicopter rotor control". pp. 158–182.

[16] Grohmann, B., Maucher, C., and Jänker, P., 2006. "Actuation Concepts for Morphing Helicopter Rotor Blades". *Proceedings of the 25th International Congress of the Aeronautical Sciences*, pp. 1–10.

[17] Leishman, J. G. "A History of Helicopter Flight".

[18] Hoagland, M. V., 1994. "Development of a Low Cost Product: The K-max Story". In 19th Congress of the International Council of the Aeronautical Sciences and the American Institute of Aeronautics Aircraft Systems Conference, AIAA.

[19] Shen, J., and Chopra, I., 2004. "Swashplateless Helicopter Rotor with Trailing-Edge Flaps". *Journal of Aircraft,* ***41***(2), pp. 208–214.

[20] Lu, Y., and Wang, C., 2015. "Active control for performance enhancement of electrically controlled rotor". *Chinese Journal of Aeronautics,* ***28***(5), pp. 1494–1502.

[21] Milgram, J., Chopra, I., and Straub, F., 1998. "Rotors with trailing edge flaps: Analysis and comparison with experimental data". *Journal of the American Helicopter Society,* ***43***(4), pp. 319–332.

[22] Yeo, H., Jain, R., and Jayaraman, B., 2016. "Investigation of rotor vibratory loads of a UH-60A individual blade control system". *Journal of the American Helicopter Society,* ***61***(3).

[23] Enenkl, B., Klöppel, V., Preißler, D., and Jänker, P., 2002. "Full Scale Rotor with Piezoelectric Actuated Blade Flaps". *28th European Rotorcraft Forum*, pp. 89.1—-X.

[24] Booth, E. R., and Wilbur, M. L., 2004. "Acoustic Aspects of Active-Twist Rotor Control". *Journal of the American Helicopter Society,* ***49***(1), pp. 3–10.

[25] Gandhi, F., and Anusonti-Inthra, P., 2008. "Skin design studies for variable camber morphing airfoils". *Smart Materials and Structures,* ***17***(1).

[26] Barbarino, S., Bilgen, O., Ajaj, R. M., Friswell, M. I., and Inman, D. J., 2011. "A review of morphing aircraft". *Journal of Intelligent Material Systems and Structures,* ***22***(9), pp. 823–877.

[27] Campanile, L. F., 2005. "Initial thoughts on weight penalty effects in shape-adaptable systems". *Journal of Intelligent Material Systems and Structures,* ***16***(1), pp. 47–56.

[28] Werter, N., Sodja, J., Spirlet, G., and De Breuker, R., 2016. "Design and Experiments of a Warp Induced Camber and Twist Morphing Leading and Trailing Edge Device". *24th AIAA/AHS Adaptive Structures Conference*(January), pp. 1–20.

[29] Cedrat, 2013. "Products catalogue version 5.1 - cedrat technologies actuator solutions".

[30] Walz, C., and Chopra, I., 1994. "Design and testing of a helicopter rotor model with smart trailing edge flaps".

[31] Zahoor, Y., De Breuker, R., and Voskuijl, M., 2020. "Preliminary design of a trailing edge morphing surface for rotorcraft". *AIAA Scitech 2020 Forum,* ***1 PartF***, pp. 1–13.

[32] Kupski, J., Zarouchas, D., and Teixeira de Freitas, S., 2020. "Thin-plies in adhesively bonded carbon fiber reinforced polymers". *Composites Part B: Engineering,* ***184***, p. 107627.

[33] Visconti, U., Eun, W. J., Sim, J. S., Lee, S. W., and Shin, S. J., 2018. "Design improvements and flap deflection evaluations with considering centrifugal load on active trailing edge flap". *Aircraft Engineering and Aerospace Technology,* ***91***(1), pp. 10–19.

[34] Leblanc, B., and Ferreira, C., 2020. "Experimental characterization of H-VAWT turbine for development of a digital twin". *Journal of Physics: Conference Series,* ***1452***(1).